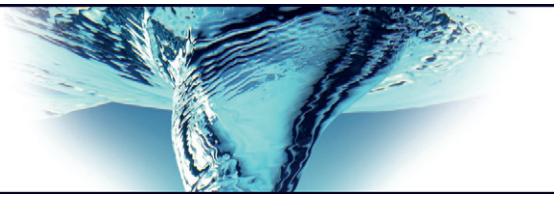
J. Fluid Mech. (2018), *vol.* 851, R6, doi:10.1017/jfm.2018.571

JFM RAPIDS
journals.cambridge.org/rapids



Vertically forced stably stratified cavity flow: instabilities of the basic state

Jason Yalim[1], **Juan M. Lopez**[1,†] **and Bruno D. Welfert**[1]

[1]School of Mathematical and Statistical Sciences, Arizona State University, Tempe, AZ 85287, USA

(Received 17 May 2018; revised 17 May 2018; accepted 14 July 2018;
first published online 31 July 2018)

The linear stability of a stably stratified fluid-filled cavity subject to vertical oscillations is determined via Floquet analysis. Retaining the viscous and diffusion terms in the Navier–Stokes–Boussinesq equations, with no-slip velocity boundary conditions, no-flux temperature conditions on the sidewalls and constant temperatures on the top and bottom walls, we find that the instabilities are primarily subharmonic (as is typical in many parametrically forced systems), except for in a few low-forcing-frequency ranges where the instabilities are synchronous. When the viscosity is small, the Floquet modes resemble the inviscid eigenmodes of the unforced problem, except in boundary layers. We establish scaling laws quantifying how viscosity regularizes the degeneracy associated with the inviscid idealization, and how it scales the thickness and intensity of the boundary layers. The product of boundary layer thickness and intensity remains constant with decreasing viscosity, leading to a delta distribution of vorticity on the walls in the limit of zero viscosity. This is in contrast to the zero wall vorticity in the inviscid case.

Key words: geophysical and geological flows, parametric instability, stratified flows

1. Introduction

Parametrically driven internal waves in a laterally enclosed container filled with an initially linearly stratified fluid have received relatively little attention compared with the study of parametrically driven interfacial waves, known as the Faraday wave problem (see the review by Miles & Henderson 1990). For the Faraday wave problem, Benjamin & Ursell (1954) showed that the linear stability of the flat-surface solution for an inviscid laterally unbounded fluid of infinite depth that is driven by a single-frequency parametric excitation reduces to the consideration of a Mathieu equation. Kumar & Tuckerman (1994) showed that viscosity introduces couplings, so that the linear stability is no longer described by a single (damped) Mathieu equation. Edwards & Fauve (1994) demonstrated experimentally that in containers of large horizontal-to-depth aspect ratios containing fluids of moderate viscosity, the

† Email address for correspondence: juan.m.lopez@asu.edu

© Cambridge University Press 2018

https://doi.org/10.1017/jfm.2018.571 Published online by Cambridge University Press

surface wave response to parametric forcing is not strongly dependent on the lateral boundaries of the container. Yih (1960), following the approach of Benjamin & Ursell (1954), showed that the linear stability of an inviscid continuously stratified and laterally unbounded fluid subjected to vertical oscillations also reduces to a Mathieu equation.

Thorpe (1968) considered the laterally bounded stratified problem. He determined the eigenmodes of a container filled with a linearly stratified inviscid fluid, as well as their leading-order nonlinear and viscous corrections, by considering small perturbations about the unforced linearly stratified state. In a rectangular container, the eigenmodes can be obtained via separation of variables and are simply products of trigonometric functions of the independent variables. In the two-dimensional case, these modes are enumerated by their horizontal and vertical half-wavenumbers, and the linear dispersion relation gives their frequency (the imaginary part of the eigenvalue; the eigenvalues are purely imaginary complex conjugates in the inviscid case) in terms of their half-wavenumbers. The inviscid eigenmodes are infinitely degenerate. Viscosity regularizes this degeneracy, but it also results in all of the eigenvalues having negative real parts, so in order to observe them in a physical setting, the system needs to be continuously forced. A number of different forcing strategies have been considered experimentally. Thorpe (1968) introduced plungers in the sidewalls of a rectangular cavity which oscillated in and out of the cavity. In this way, a number of the linear inviscid modes were observed when the plunger frequency was near to half of the eigenfrequency of the mode; only modes with the same horizontal parity as that of the forcing were excited. For large-amplitude forcing, wave breaking and mixing were observed, as well as wave beams emanating from the edges where the plungers and the sidewalls met.

Motivated to see whether the internal wave breaking could be related to triadic resonances between linear inviscid eigenmodes, McEwan (1971) constructed an experiment similar to that of Thorpe (1968), but instead of using plungers, the sidewalls were made to swing like paddles. Here too, some modes were excited, but again wave beams were generated, which compromised the comparison with the linear inviscid modes.

Orlanski (1972) conducted experiments in a rectangular container filled with linearly stratified fluid that was forced by a pair of paddles flapping on the top surface. The amplitudes of the paddle oscillations were large so that the response was nonlinear; the objective of the study was to investigate the breaking of the forced standing waves. The experiments were compared with theory and numerical simulations assuming that the flow was inviscid. General agreement between the experiments and the model results was obtained. However, secondary circulations observed in the experiments were not captured by the theory or resolved by the numerics, and this raised questions about the model assumption that the container boundaries are unimportant; the model used stress-free boundary conditions for the velocity.

The experiments of Benielli & Sommeria (1998) were groundbreaking in that they parametrically forced linearly stratified fluid in a container without any differential motion of the container walls, thus avoiding the associated generation of wave beams and secondary circulations. The forcing used was the harmonic vertical oscillation of the container, akin to the forcing used in the Faraday wave experiments. In order to observe a finite response, they needed to use a sizeable oscillation amplitude. The responses resembled the two-dimensional linear inviscid modes at early times in the experiment, but as these grew in amplitude, nonlinear effects led to wave breaking. They focused on parametrically exciting the 1 : 1 mode (eigenmode with

https://doi.org/10.1017/jfm.2018.571 Published online by Cambridge University Press

one half-wavelength in the horizontal and vertical directions). The mode appeared subharmonically, as expected, within the frequency–amplitude regime theoretically predicted to be the 1 : 1 resonance horn, but they were unable to determine the edges of the horn. Since their experiments, attention on the response to parametric forcing in contained stratified flows has shifted from exciting the container modes to studying the response to localized forcing, usually driven by a wavemaker in a corner of the container driving wave beams into the interior flow (see the reviews in Staquet & Sommeria 2002; Dauxois *et al.* 2018). This has left many open questions regarding the parametrically driven internal modes of a contained stratified flow. In this paper, we consider the linear stability problem, accounting for viscous and buoyancy diffusion effects with realistic container boundary conditions, and in particular we quantify how viscous effects (damping of modes and their harmonics, and thickness and intensity of boundary layers) scale with the ratio of the viscous time scale to the Archimedean time scale (a non-dimensional Brunt–Väisälä buoyancy frequency).

2. Governing equations and numerical techniques

We consider a fluid of kinematic viscosity ν, thermal diffusivity κ and coefficient of volume expansion β contained in a square cavity of sidelength L. The cavity sidewalls are thermally insulated, whereas the top and bottom endwalls are held at constant temperatures, T_T and T_B respectively. Gravity g acts in the downward vertical direction. In the absence of any other external forcing, the fluid is stationary with a stable linear thermal stratification. Here, we consider the stability of this system subjected to vertical harmonic oscillations with angular frequency Ω and amplitude ℓ. The Navier–Stokes equations under the Boussinesq approximation modelling the system are non-dimensionalized with length scale L, Archimedean time scale $\tau_A = 1/\sqrt{g\beta\Delta T/L} = 1/N$, where N is the Brunt–Väisälä buoyancy frequency, and temperature scale $\Delta T = T_T - T_B$. The non-dimensional governing equations in a reference frame attached to the vertically oscillating cavity are

$$\left.\begin{gathered}\frac{\partial \boldsymbol{u}}{\partial t} + \boldsymbol{u}\cdot\boldsymbol{\nabla}\boldsymbol{u} = -\boldsymbol{\nabla}P + \frac{1}{R_N}\nabla^2\boldsymbol{u} + [1+\alpha\cos(\omega t)]T\boldsymbol{e}_z, \quad \boldsymbol{\nabla}\cdot\boldsymbol{u} = 0,\\ \frac{\partial T}{\partial t} + \boldsymbol{u}\cdot\boldsymbol{\nabla}T = \frac{1}{Pr\,R_N}\nabla^2 T,\end{gathered}\right\} \tag{2.1}$$

where P is the reduced pressure, $\boldsymbol{u} = (u, w)$ is the velocity in the oscillating cavity frame, $T = (T^* - T_B)/\Delta T - 0.5$ is the non-dimensional temperature, with T^* the dimensional temperature, and $(x, z) \in [-0.5, 0.5]^2$ is the Cartesian coordinate system whose origin is fixed at the centre of the cavity. The system (2.1) is governed by four independent non-dimensional parameters: the Brunt–Väisälä number $R_N = NL^2/\nu$, the forcing frequency $\omega = \Omega/N$, the forcing amplitude $\alpha = \Omega^2\ell/g$ and the Prandtl number $Pr = \nu/\kappa$. It should be noted that $Gr = R_N^2$ is the Grashof number. We fix the Prandtl number $Pr = 1$ and consider variations in R_N, ω and α.

No-slip boundary conditions, $u = w = 0$, are imposed on all cavity walls. The top and bottom endwall temperatures are fixed, $T|_{z=\pm0.5} = \pm0.5$, and the sidewalls are insulated, $\partial T/\partial x|_{x=\pm0.5} = 0$.

The static linearly stratified state in the cavity frame of reference, i.e. the basic state,

$$\boldsymbol{u} = 0, \quad T = z \quad \text{and} \quad P = 0.5z^2[1+\alpha\cos(\omega t)], \tag{2.2a–c}$$

https://doi.org/10.1017/jfm.2018.571 Published online by Cambridge University Press

is an equilibrium solution of (2.1) for all R_N, Pr, ω and α. Linearization of (2.1) about this equilibrium state yields the system

$$\left.\begin{aligned} \frac{\partial \boldsymbol{u}}{\partial t} &= -\nabla p + \frac{1}{R_N}\nabla^2 \boldsymbol{u} + [1+\alpha\cos(\omega t)]\theta \boldsymbol{e}_z, \quad \nabla\cdot\boldsymbol{u} = 0, \\ \frac{\partial \theta}{\partial t} &= \frac{1}{Pr\,R_N}\nabla^2\theta - w, \end{aligned}\right\} \tag{2.3}$$

where $p = P - 0.5z^2[1 + \alpha\cos(\omega t)]$ is the perturbation pressure, $\theta = T - z$ is the perturbation temperature and $\boldsymbol{u}$ is the velocity perturbation away from zero. The boundary conditions are no slip for $\boldsymbol{u}$ on all walls, no flux on the sidewalls, $\partial\theta/\partial x|_{x=\pm 0.5} = 0$, and $\theta = 0$ on the top and bottom endwalls.

The governing equations (2.3) are discretized in space using a Chebyshev spectral collocation method and in time via a fractional-step improved projection scheme, incorporating the temperature equation as in Mercader, Batiste & Alonso (2010). Polynomials of degree M in both x and z are used (invariance in y is assumed), with $32 \leqslant M \leqslant 96$, depending on R_N, and 1000 time steps per forcing period $2\pi/\omega$ are used. The monodromy matrix arising from the Floquet analysis has dimension $3M^2$ and is constructed by evolving a basis for the perturbations (the corresponding identity matrix) over one period.

3. Results

We begin by recalling the linear inviscid eigenmodes of the unforced system for the square cavity (Thorpe 1968),

$$\left.\begin{aligned} \psi_{m:n}(x,z,t) &= A_\psi \sin[m\pi(x+0.5)]\sin[n\pi(z+0.5)]\sin(\sigma_{m:n}t), \\ \Theta_{m:n}(x,z,t) &= A_\theta \cos[m\pi(x+0.5)]\sin[n\pi(z+0.5)]\cos(\sigma_{m:n}t), \end{aligned}\right\} \tag{3.1}$$

where $\psi_{m:n}$ is the streamfunction, such that $(u, w) = (\partial\psi/\partial z, -\partial\psi/\partial x)$, $\Theta_{m:n}$ is the perturbation temperature, A_ψ and A_θ are the corresponding mode amplitudes, $\sigma_{m:n}$ is the eigenfrequency, and $m \geqslant 0$ and $n > 0$ are the integer half-wavenumbers. We shall refer to these inviscid eigenmodes as $I_{m:n}$. The linear dispersion relation between spatial and temporal frequencies is $\sigma^2_{m:n} = m^2/(m^2+n^2)$. It should be noted that the degeneracy $\sigma_{m:n} = \sigma_{km:kn}$ for any positive integer k; the spatial harmonics all have the same temporal frequency.

We now consider the viscous stability of the static equilibrium to parametric forcing, as described by (2.3), via Floquet analysis over the frequency range $\omega \in [0.05, 2.44]$, amplitudes $0 < \alpha \leqslant 1$ and $10^3 \leqslant R_N \leqslant 10^6$. For a given R_N, there is a critical forcing amplitude $\alpha = \alpha_c(\omega)$, which depends on the forcing frequency, below which the basic state (2.2) is stable. Over the investigated parameter range, Floquet multipliers were found to leave the unit circle through either -1 (subharmonic bifurcation, $\omega_r = \omega/2$) or $+1$ (synchronous bifurcation, $\omega_r = \omega$), where ω_r is the response frequency of the viscous Floquet eigenmode. The loci of these bifurcations, for $R_N = 2\times 10^4$, are presented in figure 1. It is only in small intervals with $\omega \lesssim 0.3$ that the synchronous bifurcation is primary. The red curve in figure 1 is the locus of synchronous bifurcations, with the tip of the 1 : 1 resonance horn indicated at $\omega \approx 0.7$, which is very close to $\sigma_{1:1} = 1/\sqrt{2}$. This is not the primary bifurcation for forcing frequency $\omega = 0.7$; the basic state (2.2) loses stability at lower α to a subharmonic Floquet mode with spatial structure resembling $I_{2:5}$ and a response

https://doi.org/10.1017/jfm.2018.571 Published online by Cambridge University Press

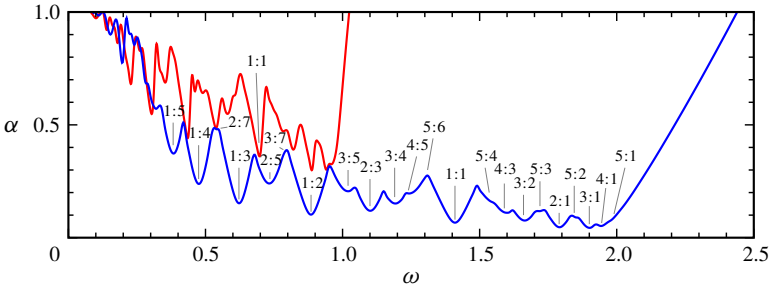


FIGURE 1. Loci of the primary subharmonic (blue curve) and synchronous (red curve) instabilities for $R_N = 2 \times 10^4$. The tips of some low-order $m:n$ resonance horns are indicated.

frequency $\omega_r = \omega/2 \approx 0.35$, which is close to $\sigma_{2:5} = 2/\sqrt{4+25} \approx 0.37$. The locus of subharmonic bifurcations is the blue curve in the figure.

In the unforced and inviscid linear theory, between any two $I_{m:n}$ and $I_{p:q}$, there exists $I_{m+p:n+q}$, which results in a Farey sequence of eigenmodes. For the forced and viscous results illustrated by figure 1, along the loci of the synchronous and subharmonic primary instabilities exist intersecting resonance horns that are associated with a finite Farey sequence of viscous eigenmodes. The bifurcating modes have m and n cells of alternating sign in the horizontal and vertical directions, and are very similar in structure to the linear inviscid unforced modes $I_{m:n}$; we shall call the viscous Floquet modes $V_{m:n}$. Figure 2 shows the spatial structure of the vorticity for some of the lower-order unforced inviscid modes, together with some intermediate higher-order modes that appear in the Farey sequence, and figure 3 shows the same for the viscous Floquet modes at $R_N = 2 \times 10^4$, $\alpha = \alpha_c$ and ω as indicated for subharmonic modes with the same $m:n$ structure as the inviscid modes in figure 2. The main difference between the inviscid and viscous modes is the presence of viscous boundary layers. Being eigenmodes, their magnitudes are arbitrary, so we have scaled the modes to have their vorticity maxima in the central region equal to 1. It is clear that the boundary layer vorticity is larger than the interior vorticity for the lower-order modes, and that the interior cells closest to the walls are distorted. Moreover, for the higher-order modes (e.g. figure 3*h* corresponding to a mode $V_{4:5}$), although the boundary layers are thinner, the viscous distortion of the cells penetrates deeper into the interior.

Within a subharmonic $m:n$ horn, the Floquet mode has half the forcing frequency, $\omega_r = \omega/2$, which is close to the corresponding frequency $\sigma_{m:n}$ of $I_{m:n}$, whereas within a synchronous $m:n$ horn, the synchronous mode has $\omega_r = \omega \approx \sigma_{m:n}$. Within a given horn, the ratio ω_r/ω is either 1 for a synchronous horn or 1/2 for a subharmonic horn, i.e. the response frequency varies within the horn, but the spatial frequencies, m and n, remain fixed.

Viscosity regularizes the degeneracy in the dispersion relation of the inviscid unforced problem. The bifurcating viscous modes are all simple (of multiplicity one), and the harmonics bifurcate in ascending order as α is increased for a given ω and R_N. That is, for modes $V_{km:kn}$, $k = 1$ bifurcates first, then $k = 2$, and so on, as α is increased. As such, the loci shown in figure 1 correspond to the bifurcations of low-order modes.

We now focus our attention on the resonance horn associated with the lowest-order mode $V_{1:1}$ that bifurcates subharmonically. It is the wide horn shown in figure 1 with

https://doi.org/10.1017/jfm.2018.571 Published online by Cambridge University Press

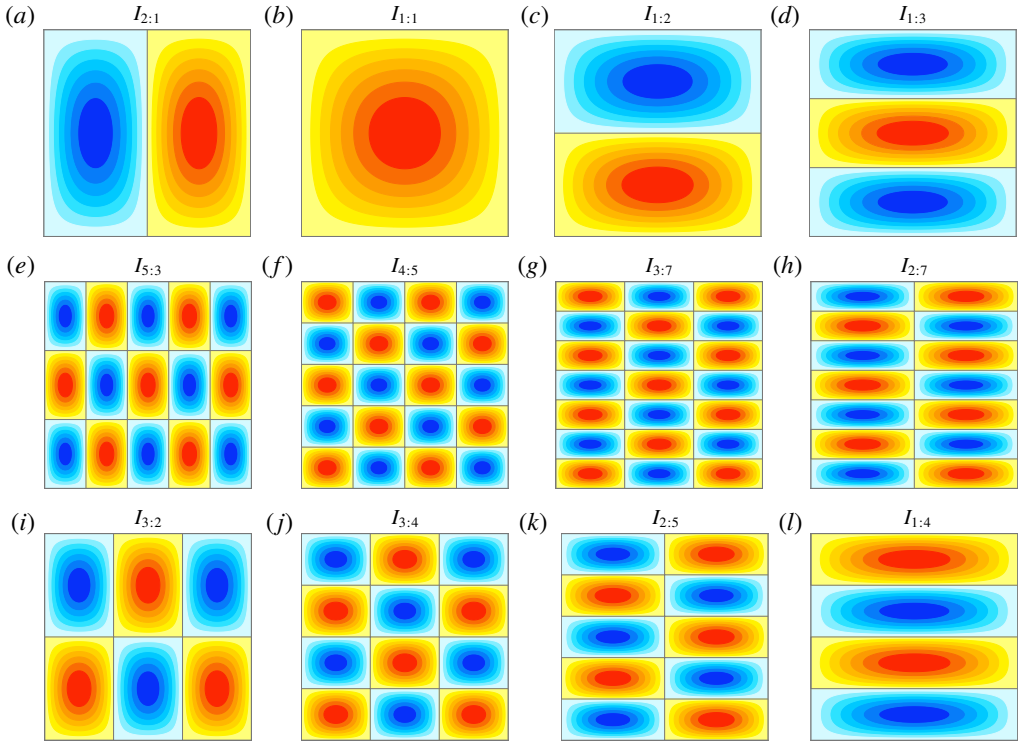


FIGURE 2. Vorticity of inviscid unforced modes with $m:n$ as indicated.

its tip at $\omega \approx 1.41$. A close-up detail of this horn is shown in figure 4(*a*), which also includes the loci of where the $V_{m:m}$ harmonics bifurcate. Within the horn, the viscous modes have exactly half the forcing frequency, $\omega/2$, which is close to the frequency of $I_{1:1}$, $\sigma_{1:1} = 1/\sqrt{2}$. It is the spatial frequency rather than the temporal frequency of the response that is locked inside the horn. The $m:m$ subharmonic resonance horns are nested one inside the other with increasing m, as illustrated in figure 4(*a*), showing the $m = 1$ to $m = 8$ horns. The tips of the horns are at $\omega_{min} \approx 1.41 \approx 2/\sqrt{2}$ and $\alpha = \alpha_{min}$. As shown in figure 4(*b*), α_{min} increases with m^2. This is an indication of how viscosity progressively dampens the higher harmonics, thus regulating the degeneracy in the inviscid idealization.

Figure 5 shows the vorticity of $I_{1:1}$ and its first seven harmonics, and the vorticity of subharmonic $V_{m:m}$, with $m \in [1, 8]$, at $R_N = 2 \times 10^4$, $\omega = 1.41$, and α slightly greater than α_c for each. Again, the most striking difference between the two sets is the presence of viscous boundary layers. For the low-m modes, the difference between the interior of the viscous mode (away from the boundary layers) and the interior of the corresponding inviscid mode is minimal, whereas, for large m, there are noticeable variations in the local vorticity maxima, indicative of viscous effects permeating deep into the interior for the higher-order modes, so that not only is their instability more viscously damped (larger α_{min} for larger m), but their structure is more viscously distorted as well.

The variations in the thicknesses of the boundary layers with m are small. Figure 4(*c*) shows that these decrease linearly with m, where the boundary layer thickness δ is taken to be the distance normal from the wall to the first zero in

https://doi.org/10.1017/jfm.2018.571 Published online by Cambridge University Press

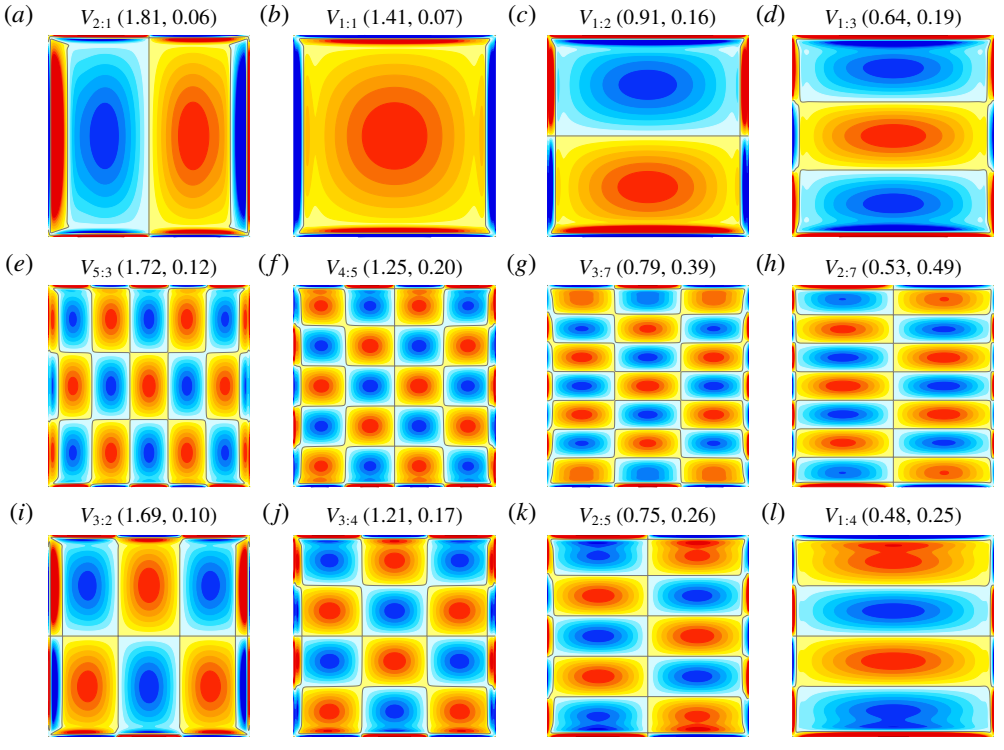


FIGURE 3. Vorticity of the leading viscous subharmonic modes along the primary instability locus for $R_N = 2 \times 10^4$ and (ω, α) as indicated.

the vorticity. The sidewall layers are thicker than the top and bottom wall layers, but they decrease faster with increasing m. Figure 4(d) shows that the ratio η_m of maximum vorticity in the boundary layer to maximum vorticity in the interior for $V_{m:m}$ diminishes with increasing m as $\eta_m = \eta_1/m$. Figure 6 shows the profiles of the vorticity in the bottom ($z = -0.5$) and sidewall ($x = -0.5$) boundary layers for the subharmonic $V_{km:km}$. Using the boundary layer scalings with m described in figure 4, these profiles collapse to a self-similar profile.

We now turn our attention to how reduction of viscous effects (by increase of R_N) acts on the subharmonic $V_{1:1}$ mode. The 1 : 1 subharmonic resonance horns for various values of R_N are shown in figure 7(a). With increasing R_N, the tip of the horn $(\omega_{min}, \alpha_{min}) \to (2\sigma_{1:1}, 0)$, with the shape of the horn approaching the V-shape that is expected for this horn in the limit $R_N \to \infty$. Figure 7(b) shows that $\alpha_{min} \propto 1/\sqrt{R_N}$. Figure 8 shows the vorticity of $V_{1:1}$ for $R_N \in [10^3, 10^6]$. The interior structure of $V_{1:1}$ is essentially equivalent to that of $I_{1:1}$, with the overall difference due to the viscous boundary layers. These boundary layers diminish in thickness as $\delta \propto 1/\sqrt{R_N}$, but their intensity increases as $\eta_1 \propto \sqrt{R_N}$, as indicated in figure 7(c,d). Using these scalings, the profiles of the vorticity in the endwall and sidewall boundary layers can be collapsed onto self-similar profiles in R_N, as shown in figure 9. The $R_N = 10^3$ profile deviates somewhat from this, indicating that for this R_N, the response is too viscous, but for $R_N > 10^4$, the response is in the asymptotic regime.

https://doi.org/10.1017/jfm.2018.571 Published online by Cambridge University Press

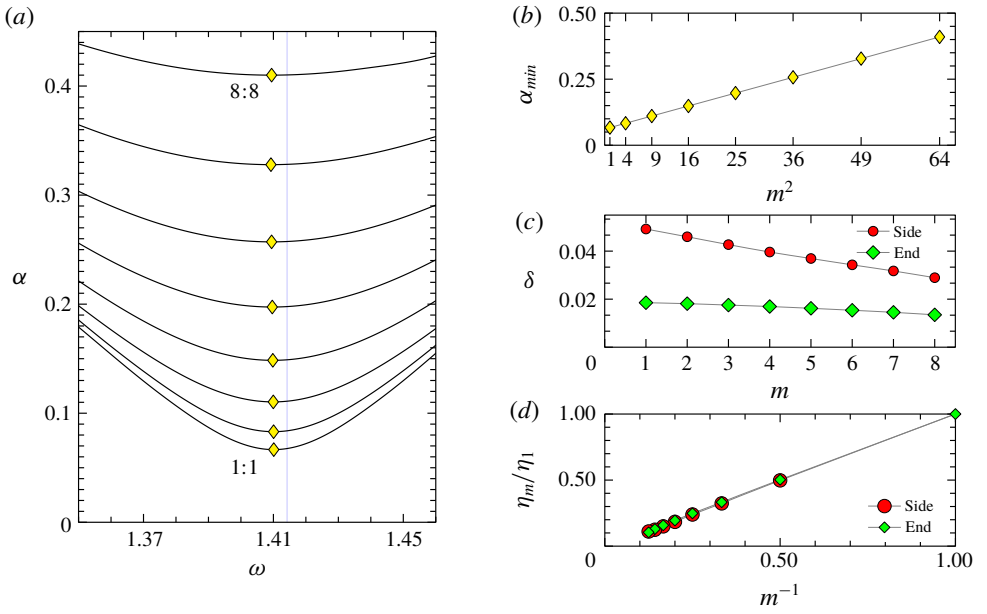


FIGURE 4. (*a*) Loci of the $m:m$ resonance horns for $R_N = 2 \times 10^4$, with m increasing sequentially from $m = 1$ to $m = 8$ with increasing α; (*b–d*) the variations of α_{min}, δ and η_m with m.

4. Conclusions

The linear stability of the static linearly stratified equilibrium in a square cavity subjected to harmonic vertical oscillations has been studied using Floquet analysis on the Navier–Stokes–Boussinesq equations with no-slip boundary conditions and zero-flux temperature conditions on the sidewalls and constant temperature conditions on the top and bottom walls. The analysis considered a large range of forcing frequencies and amplitudes, together with several decades of variation in the non-dimensional parameter R_N (the ratio of viscous to Archimedean time scales). Onset of instability was found to occur when a Floquet multiplier attained modulus greater than one as a critical forcing amplitude was exceeded at a given forcing frequency. Almost all such primary instabilities were subharmonic, with the multiplier exiting the unit circle through -1, but for a few low frequencies, the primary instability was synchronous, with the multiplier exiting through $+1$. The spatial structure of the bifurcating modes very closely resembles that of the linear inviscid modes of the unforced square cavity, differing primarily due to the presence of viscous boundary layers. As in the experiments of Benielli & Sommeria (1998), we have focused on the subharmonic $1:1$ modal response and its harmonics, at forcing frequencies in the neighbourhood of $\omega = \sqrt{2}$. We have quantified the impact of viscosity, and in particular obtained scaling laws for the critical forcing amplitude at which the harmonics become unstable, as well as scaling laws for the thickness and intensity of the boundary layers. The critical forced oscillation amplitude depends quadratically on the mode number m of the harmonic, while the boundary layer thickness and the intensity of vorticity in the boundary layer vary as $1/\sqrt{R_N}$ and $\sqrt{R_N}$ respectively, so that their product remains constant independent of R_N as $R_N \to \infty$.

https://doi.org/10.1017/jfm.2018.571 Published online by Cambridge University Press

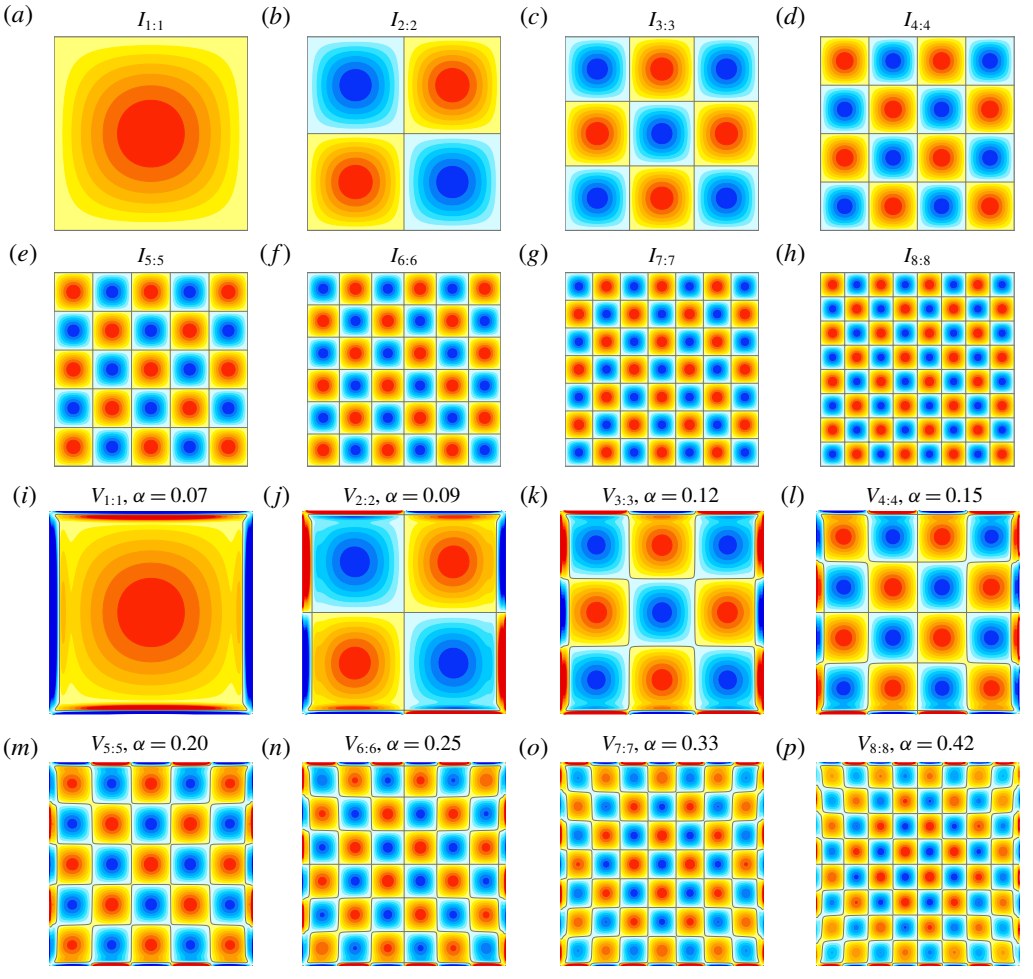


FIGURE 5. Vorticity of the first eight (*a–h*) $I_{m:m}$ and (*i–p*) subharmonic $V_{m:m}$ at $Ra = 2 \times 10^4$, $\omega = 1.41$ and $\alpha \approx \alpha_{min}$ as indicated.

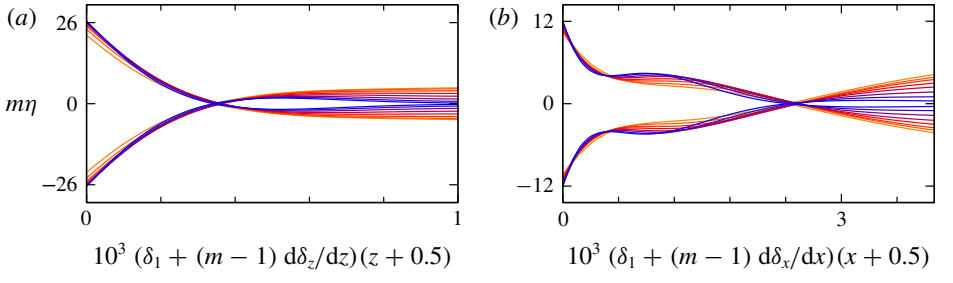


FIGURE 6. Scaled vorticity profiles at their extrema over one period of $V_{m:m}$ ($m \in [1, 8]$) at $Ra = 2 \times 10^4$, $\omega = 1.41$ and $\alpha \approx \alpha_{min}$ in (*a*) endwall and (*b*) sidewall boundary layers.

This self-similar regime is found to be attained for $Ra \sim 10^4$. This is consistent with the inviscid idealization being a singular limit as viscosity vanishes, with the lower-order viscous and inviscid modes essentially being identical in the interior

https://doi.org/10.1017/jfm.2018.571 Published online by Cambridge University Press

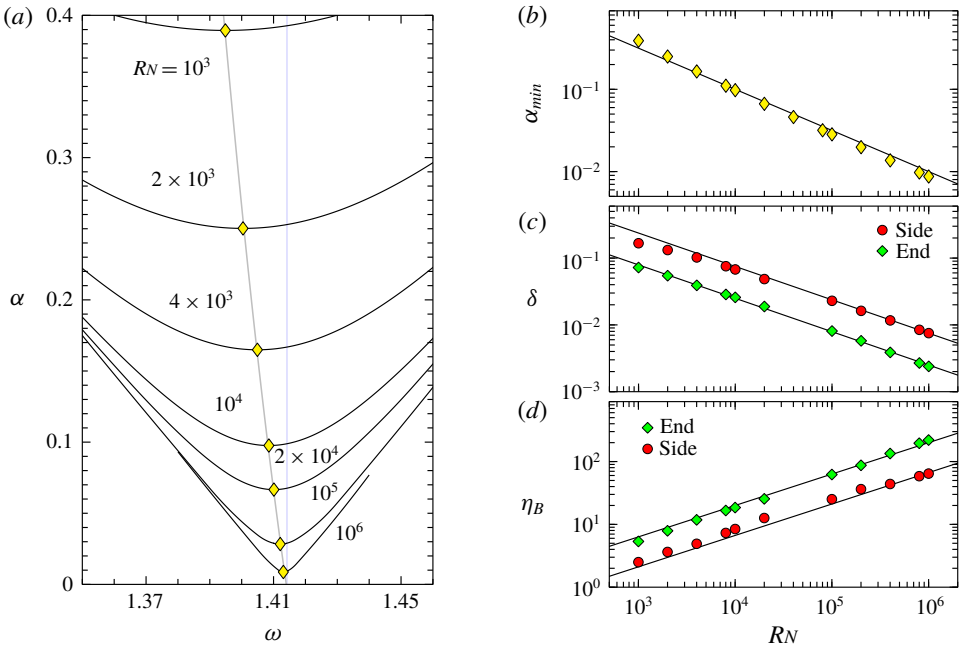


FIGURE 7. (*a*) Critical (ω, α) for subharmonic $V_{1:1}$ for R_N as indicated. The yellow diamonds are at $(\omega_{min}, \alpha_{min})$. (*b–d*) Variations with R_N of (*b*) α_{min}, (*c*) boundary layer thickness on the top/bottom walls (green diamonds) and on the sidewalls (red circles), and (*d*) ratio of interior to boundary layer maximum vorticity.

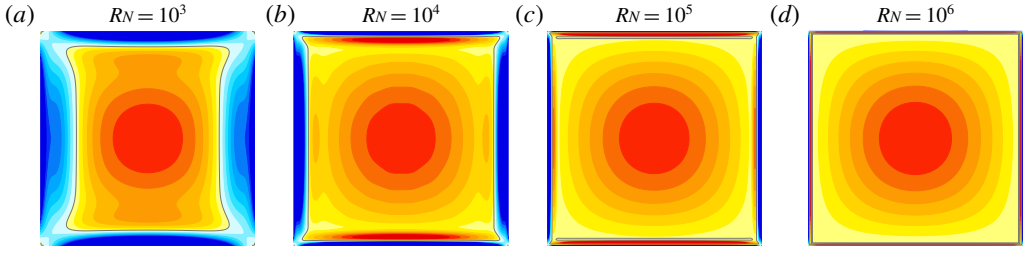


FIGURE 8. Vorticity of subharmonic $V_{1:1}$ for R_N as indicated, near $(\omega_{min}, \alpha_{min})$.

of the container. Of course, there is a major difference between the zero-viscosity approximation, which has zero vorticity at the walls, and the limit of vanishing viscosity, for which the wall vorticity is a delta distribution. At small R_N, boundary layer effects are localized near the boundaries of the container for lower modes but permeate significantly into the interior for higher-order modes, whose spatial variations in the interior are comparable in size to the boundary layer thicknesses.

It is unlikely that very-high-order modes will be observed in full nonlinear simulations or physical experiments, as low-order modes are likely to have already reached an amplitude where nonlinear effects cannot be neglected at the level of forced oscillation amplitudes needed for the high-order modes to be excited. In their experiment, Benielli & Sommeria (1998) observed low-order two-dimensional mode structures as early transients, but as their amplitudes grew, wave breaking and

https://doi.org/10.1017/jfm.2018.571 Published online by Cambridge University Press

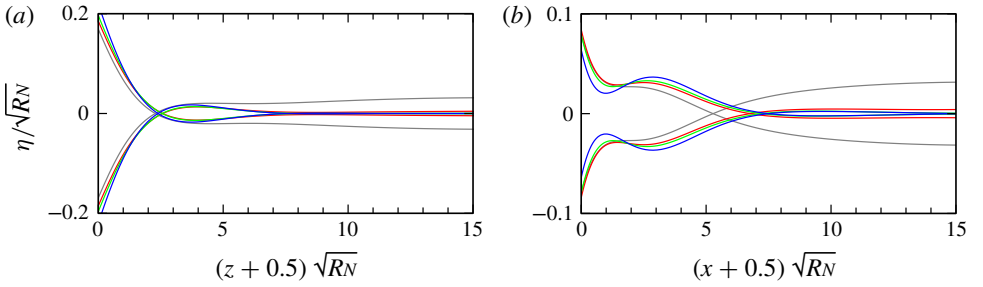


FIGURE 9. Scaled vorticity profiles in (*a*) the endwall boundary layers and (*b*) the sidewall boundary layers at their extrema over one period of subharmonic $V_{1:1}$ at the same (R_N, ω, α) as in figure 8, with $R_N = 10^3$ (grey), 10^4 (red), 10^5 (green) and 10^6 (blue).

other instabilities became dominant. The study of nonlinear mode interactions and competition beyond onset is currently being addressed.

Acknowledgements

We thank ASU Research Computing facilities and the NSF XSEDE programme for providing computing resources, and K. Wu for the original code.

References

BENIELLI, D. & SOMMERIA, J. 1998 Excitation and breaking of internal gravity waves by parametric instability. *J. Fluid Mech.* **374**, 117–144.

BENJAMIN, T. B. & URSELL, F. 1954 The stability of the plane free surface of a liquid in vertical periodic motion. *Proc. R. Soc. Lond.* A **225**, 505–515.

DAUXOIS, T., JOUBAUD, S., ODIER, P. & VENAILLE, A. 2018 Instabilities of internal gravity wave beams. *Annu. Rev. Fluid Mech.* **50**, 1–28.

EDWARDS, W. S. & FAUVE, S. 1994 Patterns and quasi-patterns in the Faraday experiment. *J. Fluid Mech.* **278**, 125–148.

KUMAR, K. & TUCKERMAN, L. S. 1994 Parametric instability of the interface between two fluids. *J. Fluid Mech.* **279**, 49–68.

MCEWAN, A. D. 1971 Degeneration of resonantly-excited standing internal gravity waves. *J. Fluid Mech.* **50**, 431–448.

MERCADER, I., BATISTE, O. & ALONSO, A. 2010 An efficient spectral code for incompressible flows in cylindrical geometries. *Comput. Fluids* **39**, 215–224.

MILES, J. & HENDERSON, D. M. 1990 Parametrically forced surface-waves. *Annu. Rev. Fluid Mech.* **22**, 143–165.

ORLANSKI, I. 1972 On the breaking of standing internal gravity waves. *J. Fluid Mech.* **54**, 577–598.

STAQUET, C. & SOMMERIA, J. 2002 Internal gravity waves: from instabilities to turbulence. *Annu. Rev. Fluid Mech.* **34**, 559–593.

THORPE, S. A. 1968 On standing internal gravity waves of finite amplitude. *J. Fluid Mech.* **32**, 489–528.

YIH, C.-S. 1960 Gravity waves in a stratified fluid. *J. Fluid Mech.* **8**, 481–508.

https://doi.org/10.1017/jfm.2018.571 Published online by Cambridge University Press